

# Effect of Interfacial Adhesion on Viscoelastic Relaxation Processes in Thin Polymer Film Indentation

Peter M. Johnson and Christopher M. Stafford\*

Polymers Division, National Institute of Standards and Technology, 100 Bureau Drive, Gaithersburg, Maryland 20899

**ABSTRACT** Polymer coatings are dependent on strongly bonded buried interfaces to maintain adhesion and protective properties over long application lifetimes. In this work, we detail the detection of buried interfaces with deviations from perfect bonded or perfect slip interfaces using surface indentation on thin films with large contact areas. The interfacial interactions between photopolymerized methacrylate films and a glass substrate were tailored using silane chemistry to create an interface that either easily releases from or cross-links with the polymer network. Creep compliance measurements on the polymethacrylate films were compared with predicted contact measurements for literature models of ideal interfaces. Nonideal contributions from interfacial effects were detected during experiments with high confinement. The extent of these effects varied with polymer network structure and polymer/substrate interface strength, with fluorinated interfaces exhibiting up to a 25% increase in indentation contact area as compared to an ideal bonded indentation due to the presence of a weak interface. The ability to probe the response of a buried interface under low indentation loads is attractive for testing and validating the interfacial properties and performance of coatings and films. This approach could be used to interrogate the fidelity of an interface in critical areas such as corrosion protection and encapsulation.

**KEYWORDS:** creep • indentation • viscoelastic properties • interfaces • adhesion • coatings

## INTRODUCTION

Viscoelastic relaxations and adhesion strength contribute to polymer performance and stability throughout an application lifetime and are controlled by the polymer network structure and dynamics, which occur over a wide spectrum of time scales. A challenge in the development and integration of complex materials interfaces lies in determining the adhesion strength of buried interfaces. Fracture methods in various geometries, such as peeling or bending, have been used to determine the adhesion and toughness of multilayered materials (1–4). The extent of deformation or force to delaminate materials can provide information about material strength, compliance, or interfacial adhesion. Recently, surface indentation techniques have received increased attention as a way to probe the local strength of materials and interfaces (5, 6). However, large indentation forces can cause complete delamination of the interface, and the delamination mechanism is dependent on the interfacial strength and indenter geometry. Here, we describe a measurement approach based on fixed load indenters to probe the interfacial properties in confined polymer films under conditions where the indentation force is significantly below the required force for complete delamination at the polymer–substrate interface.

In indentation measurements, the deformation process and resulting contact areas are controlled by the indentation geometry and material properties of the contacting solids.

The theory of contact between two elastic solids was introduced by Hertz in 1881 and describes the contact mechanics of a system with no adhesion between the contacting solids. This model has formed the classical foundation of most developed indentation techniques, ranging from the macroscale to nanoscale. Viscoelastic and soft materials, in particular, frequently deviate from Hertzian mechanics in ways that reveal critical insight into their complex properties. For example, when homogeneous contacting solids have significant adhesive forces, surface energetics between the two contacting surfaces can be invoked to account for this deviation. Models such as the Johnson, Kendall, Roberts (JKR) theory account for these effects and allow for the characterization of surface energetics or the work of adhesion between two contacting materials (2). When the indented substrate of interest is heterogeneous and composed of multiple layers of different mechanical properties, Hertzian contact mechanics fail because of different material properties in the individual layers of the substrate (7–10). In this case, indentation has been shown to measure individual layers within the substrate or an overall deformation response dependent on the indentation geometry and depth. In certain cases at much higher indentation loads, the applied stress can cause interfacial failure between the layers, resulting in a delamination indentation technique that provides information about the interfacial strength of the multilayered system (11–13).

Polymer coatings are a classic example of multilayer materials, comprising a thin polymer film on a rigid substrate. When indented, both the polymer film and underlying substrate contribute to the deformation response. A key

\* Corresponding author.

Received for review April 27, 2010 and accepted June 23, 2010

DOI: 10.1021/am100369z

2010 American Chemical Society

factor affecting the indentation response is the ratio of the contact radius,  $a$ , to the polymer film thickness,  $h$ , denoted as  $a/h$ . Within a confined regime, analytical and empirical models have been developed to account for the effect of confinement dependent on indenter geometry, with a spherical indentation of a planar surface showing significant deviations from Hertzian contact mechanics when  $a/h$  is greater than 0.1 (14, 15). In addition to the film thickness, the mechanical properties of each layer also contribute to the indentation profile, because the initial deformation response is controlled by both the polymer and substrate moduli. In the case of large moduli differences, the effects of  $a/h$  on the indentation contact area change dependent on the film thickness and the modulus difference between layers.

Although the appearance and extent of confinement effects are controlled by  $a/h$ , the stress transfer at the interface between two layers dictates the contributions of each layer to the indentation response. The adhesion strength between the two materials will either allow or inhibit polymer relaxations at an interface. Models have been developed for systems where the interface is perfectly bonded and immobile, and stress transfer occurs at the interface (16–19). The other extreme case is a perfect slip model, where the interface has no interaction effects (20, 21). For perfect slip, the film is free to translate along the surface, and the stress at the interface is considered to be zero. If both models are invoked to describe the indentation of a particular system, the perfect slip case will predict a much larger indentation deformation than the perfectly bonded model because the polymer is free to translate at the interface. In this work, we demonstrate the detection and discrimination of interfaces between perfectly bonded and perfect slip by indenting viscoelastic polymer films at loads that do not initiate film delamination. With spherical indentation of polymethacrylate films supported on glass, we show that different interfacial treatments vary the indenter response only in specific film thickness ranges dependent on the polymer network structure.

## EXPERIMENTAL SECTION

**Materials.** Equipment and instruments or materials are identified in the paper in order to adequately specify the experimental details. Such identification does not imply recommendation by the National Institute of Standards and Technology (NIST), nor does it imply the materials are necessarily the best available for the purpose. Lauryl methacrylate (LMA), isobornyl methacrylate (IBoMA), and 1,6-hexanediol dimethacrylate (HDDMA) were obtained from Sartomer (Exxon, PA). Dimethoxyacetophenone was obtained from Sigma-Aldrich (Milwaukee, WI). 3-Methacryloxypropyl dimethylchlorosilane and tridecafluoro-1,1,2,2-tetrahydrooctyl dimethylchlorosilane were obtained from Gelest (Morrisville, PA). All chemicals were used as supplied.

**Substrate Preparation.** To create interfaces close to perfect bonded and perfect slip interfaces, silane chemistry was selected to produce different functional groups on the surface of the glass slide. To imitate a perfectly bonded interface, 3-methacryloxypropyl dimethylchlorosilane was chosen to form methacrylate groups on the surface of the glass slide. Because the polymethacrylate films were photopolymerized in situ on the

modified glass slides, the methacrylate groups on the surface would cross-link with the bulk network (22). To produce a slip interface, a fluorinated silane, tridecafluoro-1,1,2,2-tetrahydrooctyl dimethylchlorosilane, was used to create a weak interface at the substrate.

To deposit a silane interface, glass slides were cleaned with toluene and ethanol, and then dried before exposure to ultraviolet light and ozone (UVO) for 500 s. Slides were then left in a toluene solution containing 10% by mass of the appropriate silane for 900 s. Slides were cleaned with toluene and water, and then dried and stored under vacuum until used. Water contact measurements were performed across the sample to confirm a uniform silane layer. In addition to polymer samples with a uniform monolayer, binary monolayer slides were produced to measure both interfaces simultaneously. To prepare these substrates, we performed different silane treatments on each half of a glass slide. Glass slides were cleaned in the same manner as above, and then half of the glass substrate was coated with deionized water and covered with a sacrificial glass slide. The silane deposition was completed in the same manner, except the silane solution never contacted the protected half of the glass slide. Once removed from the solution, the entire substrate was then rinsed and cleaned. The second silane treatment was performed, with the previously treated side covered and the other half placed into contact with the second silane for 900 s. The substrate was cleaned and dried in the same manner.

Water contact angles were measured with a drop shape analysis system (KRÜSS DSA100). Slides were used only if contact angle measurements were within the average water contact angle of  $70^\circ \pm 3^\circ$  for the methacrylate silane treatment and  $106^\circ \pm 2^\circ$  for the fluorinated silane treatment. Contact angles on binary glass substrates were statistically equivalent to single silane treatment slides. No significant differences in contact angle were seen when the order of silane deposition was reversed, and the only region with significant deviations was within a 5 mm wide boundary region between silane treatments. This boundary region was ignored and no experiments were performed in this region. Again, photopolymer methacrylate films were prepared on the binary monolayer glass substrates containing both the fluorinated and methacrylate silane as described below. Compliance measurements from binary glass substrates and singly treated glass substrates showed no significant difference.

**Film Preparation.** Two different polymer network structures were prepared for indentation measurements. All monomer formulations were prepared with 0.5% mass fraction of the photoinitiator dimethoxyacetophenone. The two monomethacrylates, LMA and IBoMA, contain pendant alkyl groups to the methacrylate functionality, and HDDMA was chosen because it is a dimethacrylate cross-linker with an alkyl center. By polymerizing with only these three monomers, alkyl and methacrylate moieties were the only chemical groups within the polymer network structure. This reduces the possibility of hydrogen bonding and limits the types of possible interactions at the interface. Three photopolymer systems were formulated, each containing LMA with a different mass fraction of comonomer. Both a high mass fraction (75% HDDMA) and low mass fraction (25% HDDMA) of dimethacrylate were copolymerized with LMA to control the cross-linking density of the network. The mass fractions were calculated based only on the monomer mass, and LMA comprised the remainder of the monomer for each formulation. The third comonomer formulation removed the cross-linking monomer and added 50% by mass fraction IBoMA (50% IBoMA) to form a linear polymer network with a glass-transition temperature close to room temperature. This network will have no gel fraction because of the lack of cross-

links, and indentations should have a greater viscoelastic response because of polymer flow over time scale of the experiment.

The monomer mixture was polymerized between two glass slides: a silane treated substrate to create the correct interfacial properties as described above, and a sacrificial superstrate with low adhesion to release and form a smooth surface for indentation. Fluorosilane treatment of the sacrificial superstrate guaranteed the polymer film would release onto the correct slide, and the indenting surface would have minimal defects. To polymerize a polymethacrylate film on a treated glass substrate, the methacrylate monomer solution was deposited between two glass slides clamped together with metal spacers at each end. Laminating between two glass slides minimized the oxygen inhibition to the dissolved oxygen present in the monomer formulation. Samples were polymerized for 3600 s using a mercury arc lamp (Acticure 2000, EXFO Systems) with a 365 nm bandpass filter at a light intensity of 10 mW/cm<sup>2</sup>. Samples were separated and left for 24 h to equilibrate in the dark before performing indentation experiments.

Film thickness gradients were produced using aluminum metal spacers having different thicknesses placed at each end of the laminated sample before clamping. The monomer solution was then wicked between the laminated slides and polymerized. The maximum height difference across a sample was 24 μm, with a maximum film thickness gradient slope of 0.30 μm/mm. An indentation with contact radius of 50 μm would have a maximum slope of 30 nm. Indentation measurements on films having thickness gradients were statistically equivalent to indentation measurements on flat polymer films, and no noncircular asperities appeared during experiments. Uncertainty in this work is displayed as the standard error from four measurements at a 95% confidence interval and includes the uncertainty from the contact radii determination. The uncertainty caused by the contact radii determination was detailed in a previous work (23).

**Indentation Design.** An indentation technique to measure bulk viscoelastic properties using optical imaging of a spherical indenter array was adapted to the indentation of thin polymer films (23). The array was modified to measure four 6.35 mm radius chrome steel spheres arranged in a row on the polymer surface. Circular holders were used to prevent any significant drift when placing spheres on the polymer film, and all four spheres were placed on the surface at the same time through the use of a vertical motion stage. The gravity load from the sphere supplied the indenting load, calculated from the mass of the indenting sphere. Contact areas were imaged with an inverted optical microscope with a translating motion stage, sequentially traveling to each contact area in the array. All experiments were performed at 22 °C, and the four spheres could be measured at intervals of 24 s. When it was necessary to collect for shorter time intervals, the number of measured contact regions was reduced to shorten time intervals. The contact geometry and experimental design are given in Figure 1.

The contact areas were imaged using an inverted optical microscope, and indentation contact radii were determined with LabVIEW image processing using edge detection and Hough transforms (23). Collected images exhibited light interference fringes around the contact area, commonly called Newton's rings. An advantage of larger radii spheres was that small changes in the indentation depth translated into significant changes in the contact area, increasing the measurement sensitivity. For the systems measured here, contact radii ranged from 30 to 100 μm, which translated into a maximum indenter penetration depth of 200 to 800 nm. The  $a/h$  parameter varied from 1.5 to 18 for the range of film thickness experiments measured. A circular Hough transform was used to calculate both a center point and a contact radius of the indenter image.

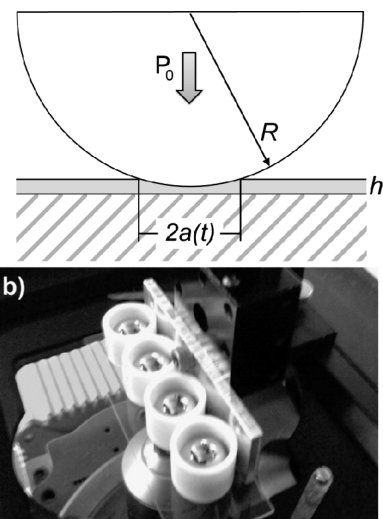


**FIGURE 1.** (a) Contact geometry for polymer film of thickness,  $h$ , on a glass substrate for constant load,  $P_0$ , indentation. The polymer film was confined between the glass slide and stainless steel indenter of radius,  $R$ , with the growth of the contact radius,  $a(t)$ , measured over time. (b) Image of four indentation setup with spheres in slotted holes to ease placement onto the polymer surface.

With the center point, the image could be transformed into a radial coordinate system, and the image data were averaged starting from the center point. This data manipulation formed an intensity plot as a function of distance from the center point. Since the center contact area displayed a constant intensity, detection of the edge of the first fringe provided the contact radius. Higher-order fringe peaks were used to confirm the accuracy of the contact radius or to detect any pile up of material at the edge of the indenting sphere. Compliance was measured up to 10000 s to determine if there were any time-scale dependent interfacial relaxations along with known polymer relaxations. After the indentation, the film next to the indentation area was scratched to measure the local film thickness.

Compliance measurements of confined films were compared with the compliance of the bulk polymer measured using the previously described indentation technique for bulk polymer samples. Bulk indentation was performed using 3 mm diameter chrome steel spheres on a 1 mm thick polymer substrate as detailed previously. Briefly, an array of nine chrome steel spheres was placed on a polymer substrate, and each point was measured and analyzed in the same manner as the indentation experiment for thin polymer films. A high magnification (20×) increased the measurement precision by increasing the pixel density of the contact areas seen in the bulk measurement, because contact areas are smaller than in the thin film indentation experiments. The contact area for bulk polymer systems exhibited smaller contact radii due to the reduced load and smaller sphere radius of the spherical indenter. Hertzian contact mechanics were valid for bulk measurements. The viscoelastic compliance for a Hertzian contact has been solved in prior work by Lee and Radok for a rigid elastic indenter and a viscoelastic substrate (24). The creep compliance,  $J(t)$ , for a step load stress response is calculated by

$$J(t) = \frac{8a(t)^3}{3RP(1 - \nu)} \quad (1)$$

where  $a$  is the contact radius,  $R$  is the indenting sphere radius,  $P$  is the load from gravity caused by the mass of the indenter, and  $\nu$  is Poisson's ratio. Poisson's ratio was set at 0.4 for all measurements. With the contact radius at each indentation

point, Hertzian mechanics were then used to determine creep compliance for each individual sphere.

**Indentation Models for Confined Polymers.** When indenting thin polymer films, the indentation stress field interacts with both the polymer film and the underlying substrate, rendering Hertzian contact mechanics invalid. For confined systems, more complex models were employed to predict contact radii based on bulk viscoelastic compliance as a function of time for each polymer network. Two models were chosen to predict contact radii for confined films, where the polymer/substrate interface was assumed to have either perfect adhesion or perfect slip. A perfectly adhered, or bonded, interface assumes no movement of the polymer film at the interface, with stress transfer at the polymer–substrate interface. Conversely, a perfect slip interface allows the polymer film to translate at the surface, and no stress is developed at the polymer–substrate interface. These assumptions of the interfacial properties simplify the indentation mechanics and allow for the model to be solved analytically under certain additional assumptions. For this work, a model for the slip interface was based on the Chadwick slip interface model (20)

$$J(t) = \frac{\pi a(t)^4}{3h_f R P (1 - \nu)} \quad (2)$$

where  $a$  is the contact radius,  $R$  is the indenting sphere radius,  $P$  is the load from gravity caused by the mass of the indenter,  $h_f$  is the polymer film thickness, and  $\nu$  is Poisson's ratio. In this case, the indenting sphere is assumed to be rigid and frictionless, and the interface between the two indented layers is frictionless slip. The underlying substrate must also be rigid, with no viscoelastic response over the time scale of the experiment.

For a perfectly bonded interface, the model based on work completed by Chen and Engel was chosen because the model was developed to work over the entire range of  $a/h$  values (15, 25). A simplified version proposed by Stevanovic et al. (17) was selected, which works for systems where the two indented layers have at least an order of magnitude difference in storage modulus. Because the modulus of the glass substrate is 65 GPa, a majority of polymer systems will fall within the acceptable range. This model parametrizes the measured contact radius at a specified film thickness to predict the Hertzian contact radius of a bulk specimen

$$a_H = \frac{a_c}{(1 - 1.04 \exp(-1.73(a_c/h)^{-0.754}))} \quad (3)$$

where  $a_H$  is the Hertzian contact radius,  $a_c$  is the measured contact radius, and  $h$  is the polymer film thickness. Using the predicted Hertzian contact radius, the compliance can be calculated with eq 1. An advantage to this model is that for large values of  $h$ , the equation simplifies to a Hertzian contact model. In our measurements, the contact radius to film thickness ratio,  $a/h$ , was kept below 16, because larger values of  $a/h$  produced insignificant changes in the contact radius in the course of the experiment. This simplified version provided a method to analyze data rapidly, but included an additional assumption where the contact area between the indenter and the underlying substrate is zero.

## RESULTS AND DISCUSSION

Photopolymer films were formed on glass slides of varying thickness for thin film indentation at different levels of

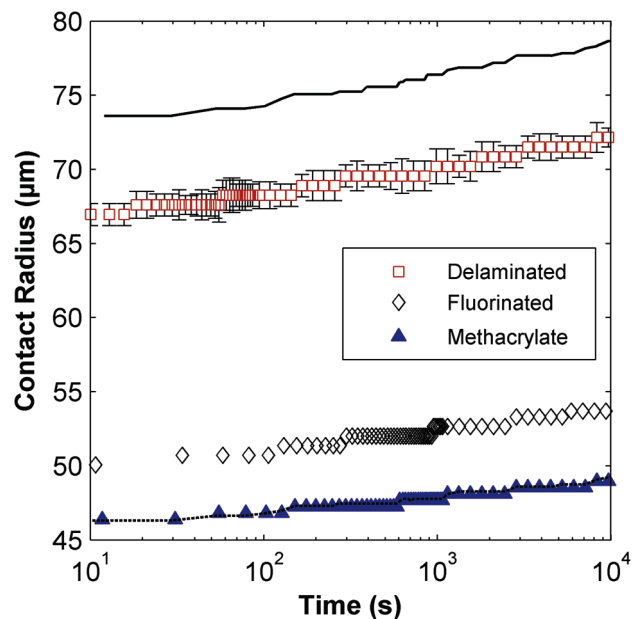


**FIGURE 2.** Contact radii measurements of a photopolymer system consisting of LMA copolymerized with 75% by mass HDDMA for a film thickness of  $19.5 \mu\text{m} \pm 0.3 \mu\text{m}$ . Indentation was with a 12.7 mm diameter steel sphere, with model predictions for perfect slip (—) and perfect bonded (---) interfaces from bulk measurements. The methacrylate interface matches the bonded bulk prediction, and error bars are not shown when smaller than the symbol size.

confinement. The highly cross-linked network, LMA copolymerized with 75% by mass HDDMA, was chosen to produce weakly adhered films on the fluorinated surface (perfect slip), or conversely, a high number of cross-links with the methacrylate silane surfaces (perfectly bonded). Indentation measurements were taken for 10 000 s on films measuring  $19.5 \mu\text{m} \pm 0.3 \mu\text{m}$  thick. To produce an interface close to the slip interface condition, the attached polymer films were removed from the fluorinated interface and placed back onto the same glass substrate. This process was done to minimize any possibilities of strongly adhered films. Fluorinated interfaces were also indented without delamination to measure any differences between an in situ polymerized interface and one that was delaminated prior to indentation. Contact radii for each interface type are shown in Figure 2, along with modeled predictions of the contact radius for both a slip and bonded interface.

As shown in Figure 2, the perfectly bonded model correctly predicted the contact radius for the confined methacrylate monolayer film from bulk measurements. The prediction agreed with the experimental contact radii throughout the entire duration of the experiment. For the slip condition of a delaminated polymer film, the predicted contact radii were significantly higher than the experimental contact radii, and the difference was maintained throughout the experiment. Because the delaminated film still must contact the surface at some point, any adhesion or stress transfer into the underlying substrate would reduce the indenter contact radius. In addition, any defects in the fluorinated interface will also contribute to deviations from a perfect slip interface. A combination of these effects reduces the contact radii to points below the idealized

perfect slip interface. Because these films show time-dependent viscoelastic relaxations, the interface will also redevelop over time and further prevent an ideal slip interface from being observed. The largest difference in contact radii was between the two experiments on the fluorinated surface. In comparison to the perfect adhesion case, the indentation contact area increased by 25% for the fluorinated interface and doubled for the delaminated interface at 120 s. When spheres are removed at short times, any deformation in the polymer film will recover back to a flat surface. The contact radii of the polymer film polymerized on the fluorinated surface were significantly lower than the contact radii from the delaminated polymer films on the fluorinated surface, providing intermediate indentation profiles between both predicted models. With a consistent polymer film thickness, the type of polymer/substrate interface was detectable based on the contact radii. For a polymer film with a methacrylate interface, the compliance of the polymer coating could be extracted from the indentation experiment, as discussed below.

Because the indentation profile changed depending on the polymer–glass substrate interface, the interfacial properties were contributing to the indentation response. To study how the properties of the polymer–glass substrate interface influenced the measured compliance, indentation experiments were performed while varying three parameters: the polymer–substrate interface, film thickness, and polymer network structure. The interfaces remained as either fluorinated or methacrylate silane glass substrates with in situ photopolymerized films. The first parameter, film thickness, controlled the extent and magnitude of the stress field at the polymer/substrate interface. Generating film thickness gradients allowed for simultaneous compliance experiments to detect when the interface ceased contributing to the indentation response. The polymer film could also be varied through formulation changes that alter cross-link density and the bulk compliance.

Both the 25 and 75% by mass HDDMA comonomer formulations were photopolymerized into film thickness gradients for indentation. Confinement effects were determined by varying the film thickness from 3 to 35  $\mu\text{m}$ , and glass substrates included either a methacrylate or fluorinated monolayer at the surface prior to polymerization. The modeled viscoelastic response is shown in Figure 3a for five different film thicknesses for the 25% by mass HDDMA copolymerization on a fluorinated glass substrate, whereas the response for a methacrylate interface is shown in Figure 3b. The compliance was calculated from the bonded interface model for all film thicknesses. Compliance should be equivalent at all points for all times if the model assumptions were accurate over the film thickness range of the experiments.

The data in Figure 3 demonstrate that polymer films above a film thickness of 11.3  $\mu\text{m}$  display equivalent compliance curves, with the two thinner films for each interface showing a higher than expected compliance. There is no significant difference for compliance measured on films thicker than 11.3  $\mu\text{m}$  ( $alh = 5.9$ ) as compared to the bulk

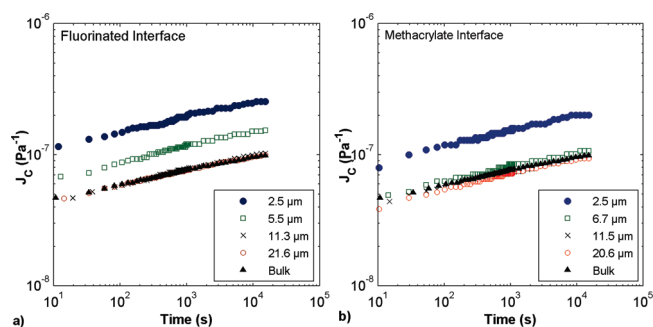


**FIGURE 3.** Compliance as calculated by the bonded model for LMA copolymerized with 25% by mass HDDMA at different film thicknesses on both (a) fluorinated and (b) methacrylate interface glass substrates. Samples above 11.3  $\mu\text{m}$  all matched bulk compliance measurements, whereas systems below this value showed higher than expected compliance. Standard error bars are smaller than sample points and are not shown for clarity.

compliance for both interfaces. In addition, the two systems at 2.5  $\mu\text{m}$  begin and end at different compliances dependent on the buried interface. For a compliance to appear higher than the bulk measurements, the contact radii must be larger than expected. Part of this deviation is caused by the assumption in the model that the contact between a glass substrate and a steel sphere is zero. The contact radius between a steel sphere and a glass slide with no polymer film was imaged and measured at  $17.3 \mu\text{m} \pm 0.33 \mu\text{m}$ . The deviation from the bonded model due to the glass indentation was significant only for very thin films, but does contribute to a larger than expected contact radius even when no deviation would be expected. This deviation from the model was present in all systems for indentations of highly confined polymer films, but contact radii measurements at equivalent film thicknesses showed significantly different contact areas.

Compliance curves on the second cross-linked network, LMA copolymerized with 75% by mass HDDMA, were generated over the same range of film thicknesses. This network contained a significantly higher amount of HDDMA, resulting in a network with higher cross-linking and a lower initial compliance than previous experiments. Deviations of greater than 10% of the bulk compliance were seen in films thinner than 15  $\mu\text{m}$  ( $alh = 3$ ) for the methacrylate interface and 25  $\mu\text{m}$  ( $alh = 2.4$ ) for the fluorinated interface. Modeled compliance for 75% by mass HDDMA formulations at different film thicknesses are given in the Supporting Information, along with contact areas and calculated compliances. Indentation on films of equivalent film thicknesses was performed on all four possible combinations of polymer and interface, with the resulting bonded model compliance shown in Figure 4. For the 75% by mass HDDMA film, the results from both interfaces were significantly different from the bulk compliance. Moreover, a significant difference in compliance was present between the fluorinated interface and the methacrylate interface, with contact radii of 52 and 47  $\mu\text{m}$  at 200 s, respectively. With a lower compliance and higher number of cross-links, the ability of the bulk polymer network to relax in the presence of an indenting load is reduced, which increases the significance of the interface.

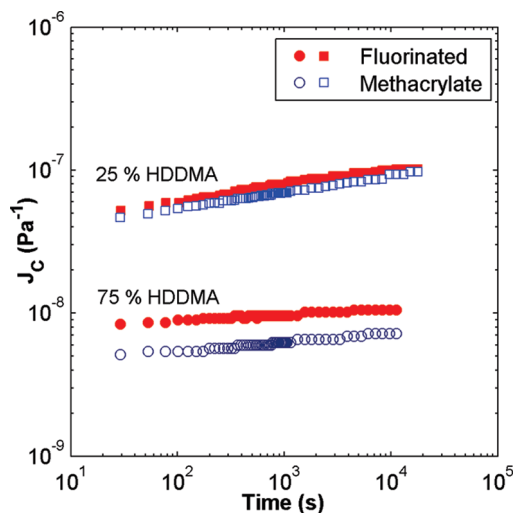


FIGURE 4. Compliance as calculated by the bonded model for sample within a polymer film thickness range of 11.2 to 11.6  $\mu\text{m}$ . Error bars are equivalent to the data point size in the figure. The 25% by mass HDDMA copolymer system exhibited a higher compliance but did not show a significant difference in compliance when the polymer and glass substrate interface was changed.

The modeled compliance for the 75% by mass HDDMA polymer network was reduced as a result of the additional cross-links, which decrease the number of polymer relaxation events available within the network. In the case of the 25% by mass HDDMA copolymer, the apparent difference was within the measured error of the experiment, and both measurements were within the error of the bulk compliance.

Because these two polymer films have different compliances, the bonded model compliance from each experiment was compared to the measured bulk compliance. This was determined using the ratio of the modeled confinement compliance to the polymer bulk compliance ( $J_c/J_{\text{bulk}}$ ) when measured at 120 s. When slip effects begin to occur or the glass substrate indentation begins to affect the model, the reduced compliance,  $J/J_{\text{bulk}}$ , will be larger than one. Comparison of the reduced compliance for both the methacrylate and fluorinated interface experiments clearly shows that contributions from the buried interface could be detected. For all systems tested, the compliance ratio was statistically equivalent to one down to a critical film thickness, at which point the ratio then increased monotonically. The reduced compliance as a function of film thickness is shown in Figure 5.

In Figure 5, the magnitude of deviations from the bulk compliance between the methacrylate and fluorinated interface changed depending on the polymer network and film thickness. All polymer films showed a deviation from bulk compliance due to the model assumption of a zero contact radii between the steel sphere and glass substrate. In the 25% by mass HDDMA copolymer, film thicknesses between 3 and 10  $\mu\text{m}$  were needed to see a significant difference in the contact radii when the polymer-glass substrate interface was modified. For the higher modulus system, the 75% by mass HDDMA copolymer, film thicknesses between 6 and 25  $\mu\text{m}$  showed significantly different responses to changes in the interfacial strength. The lower film thickness limitation

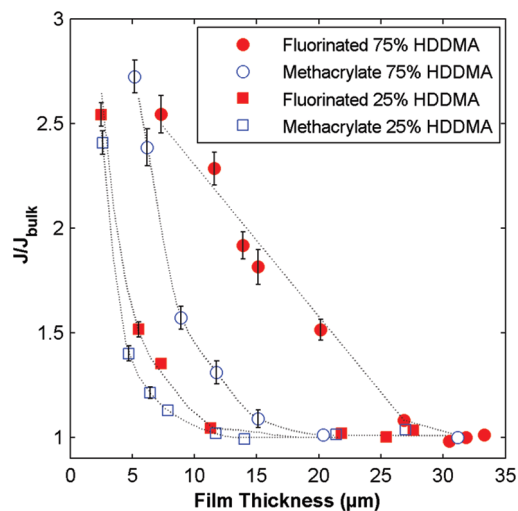


FIGURE 5. Reduced compliance at 120 s for two different polymer films, measured using indentation with either a fluorinated or methacrylate interface. LMA copolymerized with 25% by mass HDDMA ( $\square$ ) and 75% by mass HDDMA ( $\bullet$ ) by mass fraction are shown for each interface type. Compliance deviates from bulk modulus properties at different film thickness values depending on the strength of the buried interface and modulus of the film. Lines were added to guide the eye, and error bars are smaller than the size of the symbols.

was caused by contributions from the glass indentation to the indentation response, limiting the contact radii growth over time. In practice, indentation experiments where  $ah > 15$  had limited contact area growth, and compliance measurements were significantly impaired. Higher cross-link density and lower compliance provided a wider range for interface detection, because of network connectivity and limitations to the extent of polymer relaxations. In addition, interfacial contributions to the indentation response appear only below a specific film thickness, which depends both on the strength of the interface and the network structure of the polymer film.

Although cross-linked films were optimal for enhancing the interfacial effects on indentation, the compliance range measured in each experiment was limited. A linear photopolymer network with a large compliance range was prepared to determine the significance of cross-linking and increased viscoelastic relaxations. Lauryl methacrylate was copolymerized with isobornyl methacrylate to increase the modulus at room temperature and prevent adhesive effects from complicating the analysis. A formulation of LMA copolymerized with 50% by mass IBOMA was tested on both fluorinated and methacrylate treated glass substrates. This formulation was measured using indentation experiments on bulk films from 10 to 10 000 s. When polymerized, the bulk polymer compliance of this formulation at 120 s of indentation was between the two cross-linked networks. The glass transition temperature of this formulation was 37  $^{\circ}\text{C}$  as measured by differential scanning calorimetry, but photopolymerization creates a broad molecular mass distribution and a mixture of molecular weights which allow for significant relaxation (23). The compliance as a function of time for multiple film thicknesses is shown in Figure 6 for a

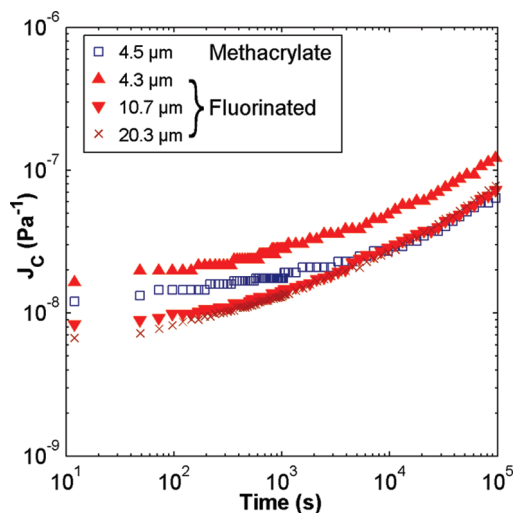


FIGURE 6. Compliance as calculated by the bonded model for a formulation of LMA copolymerized with 50% by mass IBoMA at different film thicknesses. Both the methacrylate and fluorinated interface at  $4.4 \mu\text{m} \pm 0.2 \mu\text{m}$  were shown to compare both interface types. The standard error bars are smaller than the data points, and thus are not shown for clarity.

fluorinated interface and includes a methacrylate interface measurement at a similar thickness.

In Figure 6, there is a clear difference between the fluorinated interface system at  $4.3 \mu\text{m}$  and the methacrylate interface film at  $4.5 \mu\text{m}$ . In addition to significantly different modeled compliances at 10 s, the compliance derived from the bonded model exhibits different responses over time between the two systems. The methacrylate interface exhibited an overall reduction in the creep compliance over time, eventually matching the compliance for thicker polymer films after 10 000 s. The compliance for the 10.7 and  $20.3 \mu\text{m}$  thick films on fluorinated interfaces were equivalent and similar to the compliance of the same polymer network measured from bulk indentation on 1 mm thick films (23). The deviation in modeled creep compliance over time was not equivalent for both interfaces, but the bulk polymer viscoelastic relaxation should remain constant, whereas effects at the interface change over time.

If the interfacial stress response has time-dependent behavior, these effects would be minimized in a cross-linked network because the bonding at the interface extends throughout the polymer network. If any point of a cross-linked network debonds, a large number of additional interfacial bonding points remain throughout the network. In the linear polymer network, chains not attached to the surface would relax similarly to thicker films except for the physical entanglements with chains attached to interface. Although the attached chains provided a limited resistance to relaxations and reduced the rate of creep compliance, these effects decayed as physical entanglements were removed because of polymer translation. Reduced compliance was calculated at 120 s for the linear photopolymer network to determine the film thicknesses required for interfacial detection, and is shown in Figure 7. Film thickness above  $20 \mu\text{m}$  exhibited detectable pile up around the edge of the

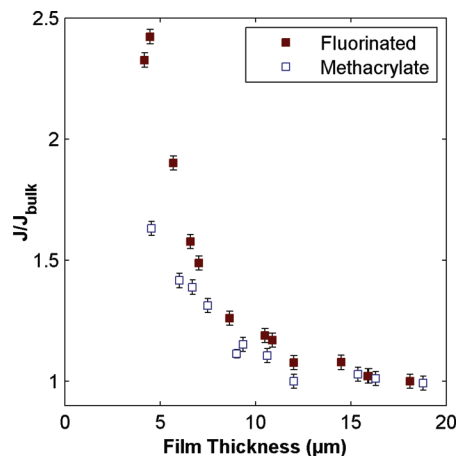


FIGURE 7. Reduced compliance at 120 s compared to bulk measurements for a formulation of LMA copolymerized with 50% by mass IBoMA. A statistically significant difference is seen between both types of interfaces when the film thickness is  $<11 \mu\text{m}$ .

indenter at long times, because the indentation contact radii grew excessively large under these conditions.

The reduced compliance for the linear systems showed a similar trend to the cross-linked systems, but the difference between the two interfaces was small until the film thickness was reduced below  $7 \mu\text{m}$ . In comparison to the cross-linked networks, the region where the interface could be detected was reduced in both magnitude and film thicknesses. Small changes in the interfacial strength would be harder to detect as well, because of the reduction of available parameter space. In all three polymer networks, the reduced compliance response from interfacial effects was different, with better discrimination between interface with increased cross-link density and lower compliance polymer networks. Because cross-linking extends the effects of the methacrylate groups bonded at the interface, these effects were consistent with the experimental results. In addition to the differences at short times, the changes in compliance at long times showed a dramatically different result. The reduced compliance calculations for long times would appear significantly different if calculated at 100 000 s instead of 120 s, but measurements at these time scales for every film thickness were beyond the scope of this paper because of time limitations. As seen in Figure 6, the methacrylate system showed a reduced compliance close to one, whereas the fluorinated sample remained well above one.

## CONCLUSIONS

For constant load indentations of confined polymer thin films, viscoelastic relaxations were influenced by both bulk viscoelastic material properties and interfacial effects under certain film thickness conditions. For the photopolymer systems shown here, the indentation response caused by interfacial effects appear within a range of film thicknesses dependent on the polymer network structure and the substrate interface. For a highly cross-linked glassy polymer network, interfacial effects were detectable when films were between 6 and  $25 \mu\text{m}$  thick. The optimal film thickness range to detect this effect decreased in width and film

thickness as the cross-link density was reduced, because network mobility and connectivity of the chemically bonded interface affected the bulk of the polymer network. In the linear polymer network, the increased mobility and the lack of cross-linked polymer chains reduced the potential film thickness range to below 7  $\mu\text{m}$ , since viscous flow outside of the interfacial region has a far greater effect on the viscoelastic compliance. With the correct film thickness, different silane glass substrate treatments at the buried interface could be detected from the indentation response as evidenced by deviations from a perfectly bonded interface. Because the bulk viscoelastic response of the polymer was consistent in an indentation of confined thin film, this technique can be used to detect different interfacial treatments for polymer coatings and determine the relative efficacy of interfacial treatments over time.

**Acknowledgment.** P.M.J. thanks the National Institute of Standards and Technology/National Research Council Postdoctoral Fellowship Program for funding. This is an official contribution of the National Institute of Standards and Technology and is not subject to copyright in the United States.

**Supporting Information Available:** Compliance data for LMA copolymerized with 75 % by mass HDDMA at different film thicknesses on both fluorinated and methacrylate interfaces, as well as contact radii at 120 s for each thickness and interface for the same system (PDF). This material is available free of charge via the Internet at <http://pubs.acs.org>.

## REFERENCES AND NOTES

- (1) Ghatak, A. *Phys. Rev. E* **2010**, *81*, 021603.
- (2) Shull, K. R.; Ahn, D.; Chen, W. L.; Flanigan, C. M.; Crosby, A. J. *Macromol. Chem. Phys.* **1998**, *199*, 489–511.
- (3) Ghatak, A.; Vorvolakos, K.; She, H. Q.; Malotky, D. L.; Chaudhury, M. K. *J. Phys. Chem. B* **2000**, *104*, 4018–4030.
- (4) Bucknall, D. G. *Prog. Mater. Sci.* **2004**, *49*, 713–786.
- (5) Kos, A. B.; Hurley, D. C. *Meas. Sci. Technol.* **2008**, *19*, 015504.
- (6) Hurley, D. C.; Kopycinska-Muller, M.; Langlois, E. D.; Kos, A. B.; Barbosa, N. *Appl. Phys. Lett.* **2006**, *89*, 021911.
- (7) Shi, X. H.; Zhao, Y. P. *J. Adhes. Sci. Technol.* **2004**, *18*, 55–68.
- (8) Johnson, K. L.; Sridhar, I. J. *Phys. D: Appl. Phys.* **2001**, *34*, 683–689.
- (9) Greenwood, J. A. *Proc. R. Soc. London, Ser. A* **1997**, *453*, 1277–1297.
- (10) Shull, K. R.; Crosby, A. J. *J. Eng. Mater. Technol.* **1997**, *119*, 211–215.
- (11) Lu, Y.; Shinozaki, D. M. *Mater. Sci. Eng., A* **1998**, *249*, 134–144.
- (12) Ritter, J. E.; Lardner, T. J.; Rosenfeld, L.; Lin, M. R. *J. Appl. Phys.* **1989**, *66*, 3626–3634.
- (13) Crosby, A. J.; Shull, K. R.; Lin, Y. Y.; Hui, C. Y. *J. Rheol.* **2002**, *46*, 273–294.
- (14) Gonda, V.; den Toonder, J.; Beijer, J.; Zhang, G. Q.; Ernst, L. J. *J. Electron. Packag.* **2005**, *127*, 33–37.
- (15) Chen, W. T. *Int. J. Eng. Sci.* **1971**, *9*, 775–800.
- (16) Matthewson, M. J. *Appl. Phys. Lett.* **1986**, *49*, 1426–1428.
- (17) Stevanovic, M.; Yovanovich, M. M.; Culham, J. R. *IEEE Trans. Compon. Packag. Technol.* **2001**, *24*, 207–212.
- (18) Giannakopoulos, A. E. *Thin Solid Films* **1998**, *332*, 172–179.
- (19) Jaffar, M. J. *J. Mech. Phys. Solids* **1988**, *36*, 401–416.
- (20) Chadwick, R. S. *SIAM J. Appl. Math.* **2002**, *62*, 1520–1530.
- (21) Conway, H. D.; Thomsin, J. P. R. *J. Adhes. Sci. Technol.* **1988**, *2*, 227–236.
- (22) Schutte, C. L. *Mater. Sci. Eng., R* **1994**, *13*, 265–323.
- (23) Johnson, P. M.; Stafford, C. M. *Rev. Sci. Instrum.* **2009**, *80*, 103904.
- (24) Lee, E. H.; Radok, J. R. M. *J. Appl. Mech.* **1960**, *27*, 438–444.
- (25) Chen, W. T.; Engel, P. A. *Int. J. Solids Struct.* **1972**, *8*, 1257–1281.

AM100369Z